Comput Visual Sci (2010) 13:265–273
DOI 10.1007/s00791-010-0143-3

REGULAR ARTICLE

A model for transport of hydrogen sulfide in oil- and water-saturated porous media

Inge Skjælaaen · Anozie Ebigbo · Magne Espedal · Rainer Helmig

Received: 21 October 2009 / Accepted: 2 September 2010 / Published online: 4 December 2010
© The Author(s) 2010. This article is published with open access at Springerlink.com

Abstract In several oilfields, reservoir souring by generation of hydrogen sulfide (H_2S) occurs in secondary recovery during which seawater is injected into originally sweet reservoirs. At the production site, high concentrations of H_2S can cause severe damage to both equipment and human personnel. Proper modeling of H_2S concentration in produced fluids can be useful for decision-making during field development design. We present a model for the transport of H_2S in an oil- and water-saturated, water-wet porous medium. The different retardation mechanisms for the H_2S are described. For the adsorption of H_2S to rock, we include two distinct phases of adsorption. In addition, we introduce a functional relationship between adsorption capacity and permeability. As H_2S mixes with oil, fractions become immobile as part of the residual oil.

1 Introduction

It is well established that the main cause of reservoir souring is the growth of sulfate-reducing bacteria (SRB) which generate H_2S. In [15], they present a one-dimensional, single-phase flow and reaction model for the transport of H_2S in a water-saturated reservoir. They simulated two basic and distinct concepts for H_2S production due to growth of SRB: (1) growth takes place in the mixing zone of injected water and formation water as introduced in [12], and (2) in a novel approach, growth takes place in biofilms close to the injection well. H_2S production profiles from field data correlated with (2) and did not match with (1). A second novelty in their model was the modeling of the adsorption of H_2S to reservoir rock which was also crucial for the model to match the field data. In [6], a model for both generation and transport of H_2S in an oil-water system is presented. In the modeling of transport, they apply a partition coefficient that depends mainly on temperature and only weakly on pressure to determine the ratio of H_2S concentration in the two phases (oil and water). In our model, we consider a water-wet porous medium which is initially oil-filled to residual water saturation and into which water containing H_2S is injected. We do not include reaction processes, i.e., we do not model the generation of H_2S. We assume that H_2S is generated by bacterial growth close to the injection well. Under the given conditions, oil and H_2S are assumed to be fully miscible, whereas a limited amount of H_2S may dissolve in water.

The objective of this paper is to present a qualitative model for the transport of H_2S in oil reservoirs, describing the different retardation mechanisms separately and in relation with the mathematical model. Comparing numerical results with field data is beyond the scope of this article as we perform only qualitative sensitivity tests for explanatory purposes. For a discussion on industrial applications of reservoir souring models, see [5].

In Sect. 2, we present the physical concept of the model. In Sect. 3, we present the mathematical model, and in Sects. 4 and 5, we describe the different retardation mechanisms. In Sect. 6, we briefly explain the numerical solution approach.

Communicated by Gabriel wittum.

This article is dedicated to the memory of our dear colleague, friend and mentor, Magne Espedal, who passed away during the preparation of this manuscript.

I. Skjælaaen (✉) · M. Espedal
Centre for Intregrated Petroleum Research,
Unifob, Norway
e-mail: inge@skjaelaaen.com

A. Ebigbo · R. Helmig
Department of Hydromechanics and Modeling of Hydrosystems,
University of Stuttgart, Stuttgart, Germany

In Sect. 7, we present sensitivity test examples, and concluding remarks are given in Sect. 8.

2 Physical model

Following the conclusions in [15], we assume that the sulfate-reducing bacteria (SRB) are able to live and reproduce, and hence generate H_2S, only close to the injection well. The computational domain is defined such that the direction of production is from West to East, i.e., there is inflow at West and outflow at East. At the West boundary, there is inflow of H_2S and inside the domain there is no source/production of either H_2S or SRB. We assume no temporal or spatial variation for the temperature within the computational domain. The porous medium is assumed to be water-wet and initially oil-saturated up to residual water saturation. At the West boundary of the computational domain, the oil saturation is assumed to be zero such that the inflow is water containing H_2S. We assume that H_2S and oil are miscible at reservoir conditions, hence H_2S does not form a separate phase.

3 Mathematical model

Here we present the mathematical setup for our specific model. For general multiphase multicomponent models, see e.g. [14].

The phases are oil (o) and water (w), and the components are oil, water and hydrogen sulfide, H_2S, for simplicity denoted by (g). We define $\alpha = (o, w)$ and $i = (o, w, g)$. For the phases α, we define the relative permeability $k_{r\alpha}$, the viscosity μ_α, the pressure p_α, the density ρ_α and the saturation S_α. The absolute permeability tensor is denoted by $\mathbf{K}$. We assume that the variance in depth of the reservoir is small enough to set the gravitational acceleration $\mathbf{g}$ as a constant. The Darcy velocity $\mathbf{u}_\alpha$ for the phase α is then

$$\mathbf{u}_\alpha = \frac{k_{r\alpha}}{\mu_\alpha}\mathbf{K}(\nabla p_\alpha - \rho_\alpha \mathbf{g}). \tag{1}$$

We define the diffusion coefficient d_α^i for component i in phase α and the tortuosity τ_α which is a measure for the irregularity of the flow paths. Using the approach introduced in [13], it is defined by

$$\tau_\alpha = \frac{(\phi S_\alpha)^{7/3}}{\phi^2}. \tag{2}$$

The diffusion tensor $\mathbf{D}_\alpha^i$ for the component i in phase α is then given by

$$\mathbf{D}_\alpha^i = \tau_\alpha \phi S_\alpha d_\alpha^i \mathbf{I}, \tag{3}$$

where $\mathbf{I}$ is the $m \times m$ identity matrix. m is the number of spatial dimensions.

We define

$$N_i = \sum_{\alpha=o,w} \rho_\alpha X_\alpha^i S_\alpha \tag{4}$$

and

$$F_i = \sum_{\alpha=o,w} \rho_\alpha \mathbf{u}_\alpha X_\alpha^i, \tag{5}$$

where X_α^i is the mass fraction of component i in phase α. We define the amount A_i of adsorbed mass of component i to rock. This is discussed in Sect. 5. Finally, porosity ϕ is assumed to be constant in time, so that we have for $i = (w, o, g)$ the following mass balance equation:

$$\phi \frac{\partial (N_i + A_i)}{\partial t} + \nabla \cdot (F_i(p, T)) - \sum_\alpha \nabla \cdot \left(\mathbf{D}_\alpha^i \rho_\alpha \nabla X_\alpha^i\right) = 0. \tag{6}$$

Equation (6) represents three equations. In the case that both phases are present (other cases are discussed in Sect. 6.1), we solve Eq. (6) for the independent variables S_w, p_o and X_o^g. To close the system, we need to determine the secondary variables as functions of the primary variables. First, we have that the saturations must satisfy

$$S_w + S_o = 1. \tag{7}$$

We have the capillary pressure relation

$$p_c = p_o - p_w, \tag{8}$$

where the capillary pressure is set to be a function of the water saturation, $p_c = p_c(S_w)$. Relative permeability is also a function of saturation, $k_{r\alpha} = k_{r\alpha}(S_\alpha)$. The densities and viscosities may be functions of pressure and temperature, $\rho_\alpha = \rho_\alpha(p_\alpha, T)$ and $\mu_\alpha = \mu_\alpha(p_\alpha, T)$.

Further, we need functional relations between the mass fractions, relations through which important dynamics are modeled in our work. This is explained in the Sect. 4.

4 Equilibrium equations

The mass fractions of the components oil and water in the water and oil phases, respectively, are set to be functions of thermodynamical variables $\mathbf{T} = (p_o, p_w, T)$:

$$X_w^o = f_1(\mathbf{T}), \tag{9}$$

and

$$X_o^w = f_2(\mathbf{T}). \tag{10}$$

The absorption of H_2S in oil and water is modeled through the determination of the mass fractions of H_2S in the two phases, and is explained in Sect. 4.1.

4.1 Partitioning of H_2S

The total amount of H_2S present is assumed to be instantaneously distributed in oil, water, and the surface of the rock, i.e., kinetics are not modeled. This is justified by the large ratio between the mass transfer velocities and the flow velocities. We explain the distribution of H_2S in the case where both phases are present, i.e., when X_o^g is a primary variable. The solubility of H_2S in water is calculated using Henry's law:

$$X_w^g = \frac{X_o^g p_o}{K_H(T)} \tag{11}$$

where $K_H(T)$ is the Henry constant given by [3,10]:

$$\log K_H(T) = 84.44 + 0.0101845T - \frac{3.792 \times 10^3}{T} - 29.5008 \log(T) \quad [\text{MPa}], \tag{12}$$

where T is in K. The sum of mass fractions in one phase must satisfy

$$\sum_i X_\alpha^i = 1, \tag{13}$$

hence with the definitions above, all mass fractions are defined, and the system of equations is closed in a REV in which both phases are present. On the other hand, when only one of the phases is present, a change in the set of primary variables is necessary. This is explained in Sect. 6.1.

5 Adsorption

A fraction of the H_2S gets adsorbed by the rock. Water being the wetting phase in our model, we assume that the rate of adsorption of H_2S at the rock surface is a function of the concentration of H_2S in water and not directly dependent on X_o^g. The amount A_g of adsorbed H_2S is then a function of X_w^g and of thermodynamical variables:

$$A_g = A_g(X_w^g, \mathbf{T}). \tag{14}$$

Note that no other adsorption processes are considered here, i.e., $A_w = A_o = 0$. An adsorption capacity C^r for the rock should define an upper limit for A, and A should increase with increasing X_w^g. A simplistic approach to the adsorption function is:

$$A_g = C^r \frac{X_w^g}{k + X_w^g}, \tag{15}$$

where $k = k(\mathbf{T})$ is a function of thermodynamical variables. It is the value of X_w^g at which half the adsorption capacity is reached. Note that in this approach, A_g is a Langmuir isotherm [11], i.e., no kinetics are involved in the modeling of the adsorption. In [15], it is emphasized that no isotherm can satisfy all the properties one would expect from the adsorption of H_2S at the rock, since the isotherm only depends on the concentration of H_2S in the fluid and does not take into account the amount of currently adsorbed H_2S. They point out that the adsorption process consists of two phases, the first of which has a higher affinity and lower capacity than the second. To approach the distinction of the two phases of adsorption, we define two adsorption functions $A_1(X_w^g, k_1, C_1^r)$ and $A_2(X_w^g, k_2, C_2^r)$ for the first and the second phase, with $C_1^r < C_2^r$ and $k_1 < k_2$, see Fig. 1. For a given set of parameters and H_2S concentration in water, A is then chosen such that $A = \max(A_1, A_2)$.

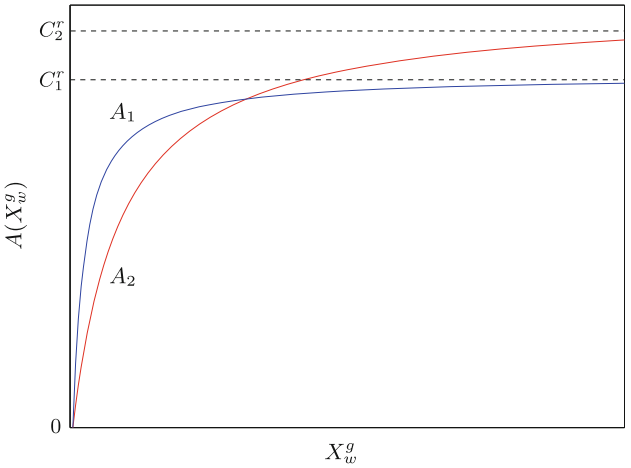

Fig. 1 Adsorption functions A_1 and A_2 for the two adsorption phases

5.1 Adsorption capacity related to permeability, porosity and surface area

The adsorption capacity is related to the surface area of the reservoir rock. It is not straightforward how to include this relation in a Darcy-scale model, and here we present our approach. In *Kozeny's equation*, porosity ϕ, surface area M and permeability K (here considered a scalar) are related by:

$$K = c \cdot \frac{\phi^3}{M^2} \tag{16}$$

where c, called *Kozeny's constant*, varies with the geometrical shape of the pore channels [2]. We define reference values ϕ_0, M_0, and K_0 at a point (x_0, y_0), and have that

$$\frac{K}{K_0} = \left(\frac{\phi}{\phi_0}\right)^3 \left(\frac{M_0}{M}\right)^2. \tag{17}$$

To reduce the degrees of freedom, we assume that changes in ϕ are much smaller than changes in K or M and neglect its effect in the equation. We therefore have

$$K = K_0 \left(\frac{M_0}{M}\right)^2. \tag{18}$$

Finally we relate the adsorption capacity with the surface area by

$$C_1^r = C_{1,0}^r \frac{M}{M_0}, \qquad C_2^r = C_{2,0}^r \frac{M}{M_0}. \tag{19}$$

6 Numerical model

We use the numerical simulator MUFTE-UG, developed at University of Stuttgart and University of Heidelberg see [1,8]. UG is a general platform for solving partial differential equations, and the MUFTE part is where the discretized equations are specified. The latter is briefly explained in the following. A fully implicit Euler scheme is applied for the storage term. For spatial discretization, the BOX method [7] is applied. The BOX method is locally mass conservative and can be used for unstructured grids. For stable and non-oscillating solutions, a fully upwind technique is applied for the advection term, whereas non-physical spatial oscillations are avoided by the *mass lumping technique* [9]. The non-linear system of three coupled partial differential equations is linearized by the *Newton-Raphson method*, and *line search* is carried out to evaluate the need for time step reduction.

6.1 Adaptive choice of primary variables

As Eq. (6) represents three independent equations, we have to determine three independent primary variables in order to describe the thermodynamical state of the system. The choice of the primary variables must be consistent with the phase state. It must be possible to calculate all secondary variables from the primary variables. For instance, if only water is present then the amount of H_2S in water cannot be calculated through the amount of H_2S in oil, hence X_w^g must be a primary variable, and accordingly for X_w^o. The primary variables are switched when the solution for the current set of primary variables becomes non-physical. For example, given a situation in which both phases are initially present, one of the two phases may disappear if the solution for its saturation becomes negative. In this case, the initial primary variable, i.e., the saturation, is replaced by the mass fraction of that component in the phase which is still present. In a single-phase system, on the other hand, the appearance of a second phase is warranted if the mass fraction of a component in the phase exceeds its solubility limit. In this case, the mass fraction is substituted by a saturation as the primary variable. In Table 1, the different phase states and the corresponding sets of primary variables are listed.

Table 1 Phase states and corresponding primary variables

Phase state	Phases present	Primary variables
Oil phase	Oil (o)	X_o^w, p_o, X_o^g
Water phase	Water (w)	X_w^o, p_w, X_w^g
Both phases	w, o	S_w, p_o, X_o^g

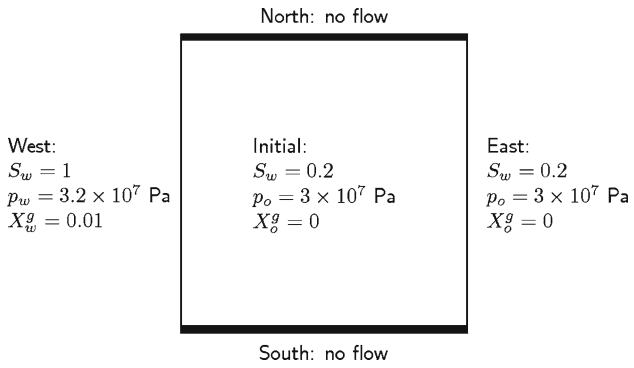

Fig. 2 Boundary and initial conditions for the standard case simulation

For a schematic overview of the algorithms and more on the switch in primary variables, see e.g. [4].

7 Simulations

Here, we present a qualitative sensitivity test study. The reservoir is small and two-dimensional, 10×10 m^2, for the sake of computational efficiency. First, we show a standard case simulation for which the boundary conditions, the initial conditions and the parameters are given in Table 2 and Fig. 2. Water is injected into an initially oil-filled (i.e., residually saturated with water) and H_2S-free reservoir. This is achieved by setting constant values at the western and eastern boundaries, while the northern and southern boundaries are assumed to be impermeable. The conditions at the East are identical to the initial conditions. At the West, inflow of water is ensured by assigning a higher pressure at the boundary than within the domain and, assuming that the boundary is sufficiently near to the injection well, a water saturation of unity. The water entering the domain is assumed to contain a given amount of H_2S produced by bacteria near the injection well – hence $X_w^g = 0.01$ is set at the western boundary.

The results are presented in Fig. 3, where the flux of oil, water and H_2S at the East boundary, i.e., close to production well, are plotted as a function of time. We see that the water breakthrough takes place after three days, while H_2S is not produced before the the eleventh day, approximately. This retardation of the transport of H_2S within the domain is caused by the mixing of the H_2S with the residual oil and adsorption at the surface of the rock. The parameters which control the character of the simulation results are the

Table 2 Standard case setup

Parameters						
Temperature				363.15 K		
Porosity				0.15		
Absolute permeability				2.0×10^{-14} m^2		
Residual water saturation, S_{wr}				0.2		
Residual oil saturation, S_{or}				0.2		
Density water				1100 kg/m^3		
Density oil				750 kg/m^3		
Viscosity water				0.5534×10^{-3} Pa·s		
Viscosity oil				1.0322×10^{-3} Pa·s		
Solubility oil in water, X_w^o				0		
Solubility water in oil, X_o^w				0		
Adsorption capacities; first phase C_1^r, second phase C_2^r				$C_1^r = 2,\ C_2^r = 2.4$ kg/m^3		
Adsorption function coefficients, $k_1,\ k_2$				$k_1 = 4.5 \times 10^{-4},\ k_2 = 4k_1$		
Diffusion coefficient $d_o^{H_2S}$				1.0×10^{-9} m^2/s		
Diffusion coefficient $d_w^{H_2S}$				1.0×10^{-9} m^2/s		
p_c-S_w relationship				van Genuchten: $p_c = \frac{1}{\alpha}\left(S_e^{-1/m} - 1)^{1/n}\right)$ $m = 1 - 1/n$ $S_e = \frac{S_w - S_{wr}}{1 - S_{wr} - S_{or}}$, for $1 - S_{or} > S_w > S_{wr}$		
α				2.8×10^{-4}		
n				1.67		
Relative permeability, water				van Genuchten: $k_{rw} = \sqrt{S_e}\left[1 - \left(1 - S_e^{1/m}\right)^m\right]^2$		
n				1.67		
Relative permeability, oil				van Genuchten: $k_{ro} = \sqrt{1 - S_e}\left[1 - S_e^{1/m}\right]^{2m}$		
n				1.67		
Boundary conditions						
Boundary	Type	State	Variable	Value	Unit	Comment
West	Dirichlet	Water phase	X_w^o	0.0	–	
			p_w	3.2×10^7	Pa	
			X_w^g	0.01	–	
East	Dirichlet	Both phases	S_w	0.2	–	
			p_o	3.0×10^7	Pa	
			X_o^g	0.0	–	
North	Neumann	Both phases	q_w	0.0	kg/m^{2}s	no flow (water)
			q_o	0.0	kg/m^{2}s	no flow (oil)
			q_{H_2S}	0.0	kg/m^{2}s	no flow (H_2S)
South	Neumann	Both phases	q_w	0.0	kg/m^{2}s	No flow (water)
			q_o	0.0	kg/m^{2}s	No flow (oil)
			q_{H_2S}	0.0	kg/m^{2}s	No flow (H_2S)
Initial conditions						
Variable			Value		Unit	
S_w			0.2		–	
p_o			3.0×10^7		Pa	
X_o^g			0		–	
Phase state			Both phases		–	

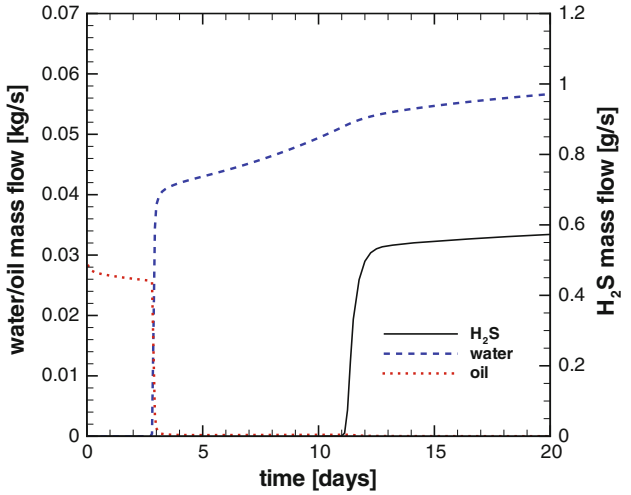

Fig. 3 Fluxes of oil, water and H_2S at production for the standard case simulation

residual oil saturation, the adsorption capacity of the rock and the amount of H_2S flowing into the domain. In the following, simulations conducted in order to study the variation of these parameters are presented. Finally, we present a test case with a heterogeneous permeability field which affects the adsorption capacities through the effective rock surface area. The results from all simulations are compared with the standard case.

7.1 Variation of the residual oil saturation

As oil mixes with H_2S from the injected water, a fraction of the H_2S will remain in the residual oil. The higher the residual oil saturation, the more H_2S is immobilized as it mixes with the residual oil. In the standard case, $S_{or} = 0.2$. In Fig. 4a, results for $S_{or} = 0.1$ show a later water breakthrough than in the standard case due to the larger amount of pore space available for the water phase. On the other hand, H_2S breaks through earlier since the capacity of immobilization due to mxing with residual oil is reduced. Accordingly, in Fig. 4b, where $S_{or} = 0.4$, the water breakthrough takes place earlier, and H_2S reaches the production site later.

7.2 Variation of the adsorption capacity

In Fig. 5a, the adsorption capacities are halved compared to the standard case such that $C_1^r = 1$ kg/m^3 and $C_2^r = 1.2$ kg/m^3. We see that water breakthrough has not changed from the standard case (which is obvious since the flow of water is not depndent on the adsorption of H_2S), but the H_2S reaches production faster than in the standard case since a smaller amount of H_2S can be immobilized due to adsorption. When doubling the adsorption capacities such that $C_1^r = 4$ kg/m^3 and $C_2^r = 4.8$ kg/m^3, we see from Fig. 5b that H_2S reaches

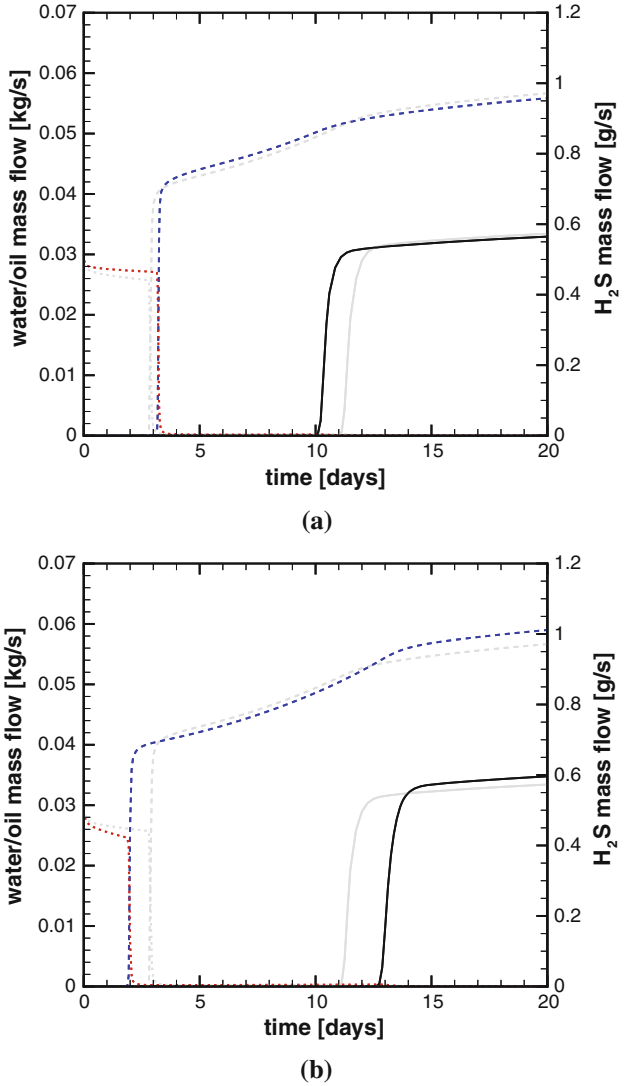

Fig. 4 Fluxes of oil, water and H_2S at production for different residual oil saturation values. The *continous line* represents the H_2S flux, the *dashed line* is the water flux, and the oil flux is depicted with the *dotted line*. The results of the standard case simulation are shown in *gray*. **a** Lower residual oil saturation, $S_{or} = 0.1$. **b** Higher residual oil saturation $S_{or} = 0.4$

production much later than in the standard case, while water breakthrough is not changed. In both cases, the adsorption function parameters k_1, k_2 (see Sect. 5 and Table 2) are not changed from the standard case.

Note that the changes in residual oil saturation and adsorption capacity have a very limited effect on the flux of H_2S after breakthrough (i.e., at steady state).

7.3 Variation of rate of H_2S generation

In Fig. 6, results from simulations with lower and higher amounts of H_2S in the injected water, are shown. In the case resulting in Fig. 6a, the mass fraction of H_2S in water at

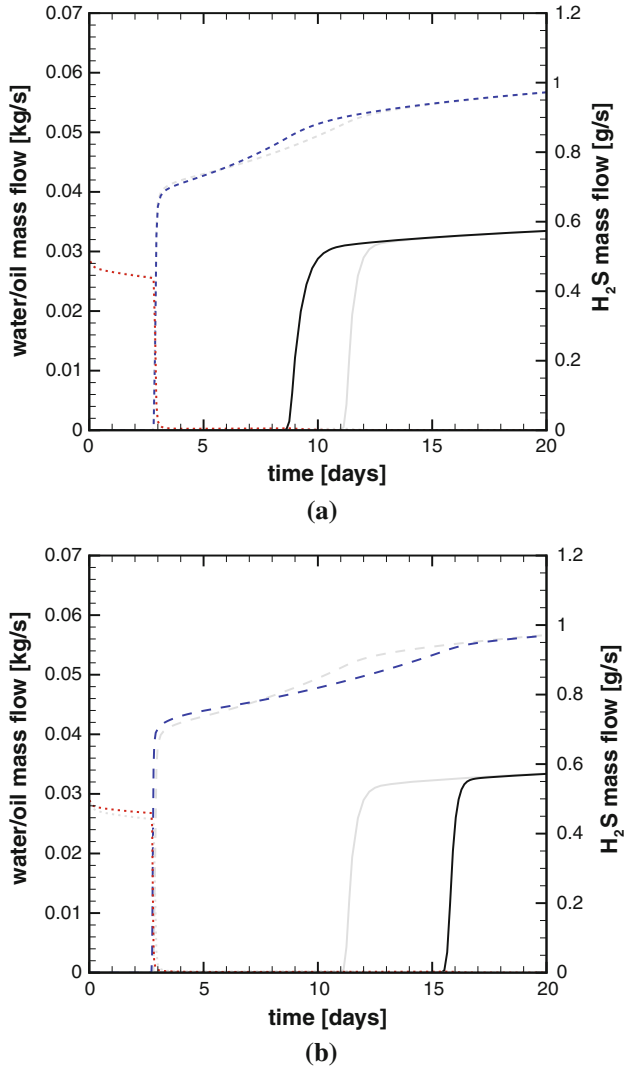

Fig. 5 Fluxes of oil, water and H_2S at production for different sets of adsorption capacities. The *continous line* represents the H_2S flux, the *dashed line* is the water flux, and the oil flux is depicted with the *dotted line*. The results of the standard case simulation are shown in *gray*. **a** Lower adsorption capacities, $C_1^\tau = 1, C_2^\tau = 1.2$. **b** Higher adsorption capacities, $C_1^\tau = 4, C_2^\tau = 4.8$

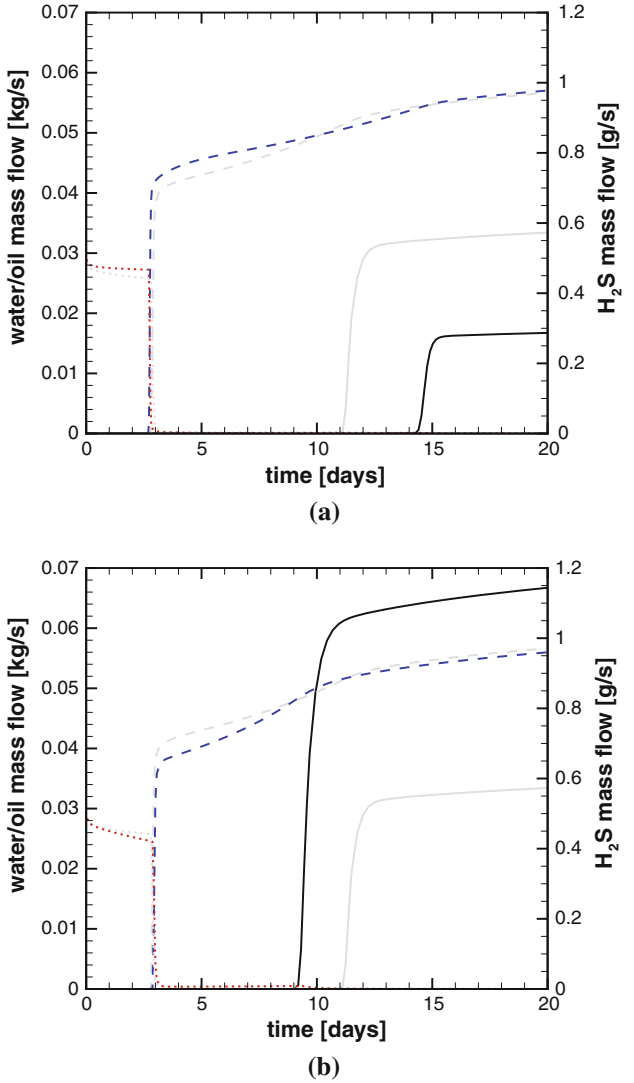

Fig. 6 Fluxes of oil, water and H_2S at production for different amounts of injected H_2S. The *continous line* represents the H_2S flux, the *dashed line* is the water flux, and the oil flux is depicted with the *dotted line*. The results of the standard case simulation are shown in *gray*. **a** Lower H_2S injection, $X_w^g = .05$. **b** Higher H_2S injection, $X_w^g = .2$

injection is halved compared to the standard case such that $X_w^g = 0.05$. We see that H_2S reaches production later than in the standard case, and that the flux is also lower, both as expected. In Fig. 6b, results from doubling the mass fraction of H_2S in water at injection are shown. As expected, H_2S reaches production earlier and with a higher flux than in the standard case.

7.4 Heterogeneous permeability field

Here, we present a simulation in which the permeability field is heterogeneous; see Fig. 7a. All other parameters and initial conditions are as in the standard case. In Sect. 5.1, relations between porosity, rock surface area and adsorption capacity are explained. The values for $C_{1,0}^r$ and $C_{2,0}^r$ are identical those of C_1^r and C_2^r, respectively, of the standard case simulation. In the given field, the total adsorption capacity of the domain is equal to that of the standard case simulation.

In Fig. 7b, c, the distribution of adsorbed H_2S by the rock after 6 and 20 days, respectively, is shown. As expected, the amount of adsorbed H_2S is low in high permeable zones, and high in low permeable zones. Between the extrema, the permeability field and the adsorption distribution field are not linearly related. In Fig. 8, we see that, due to preferential pathways, the water front as well as the H_2S front are not as sharp as in the standard case. In addition, since less H_2S gets adsorbed in high permeable zones (see Fig. 7b) through

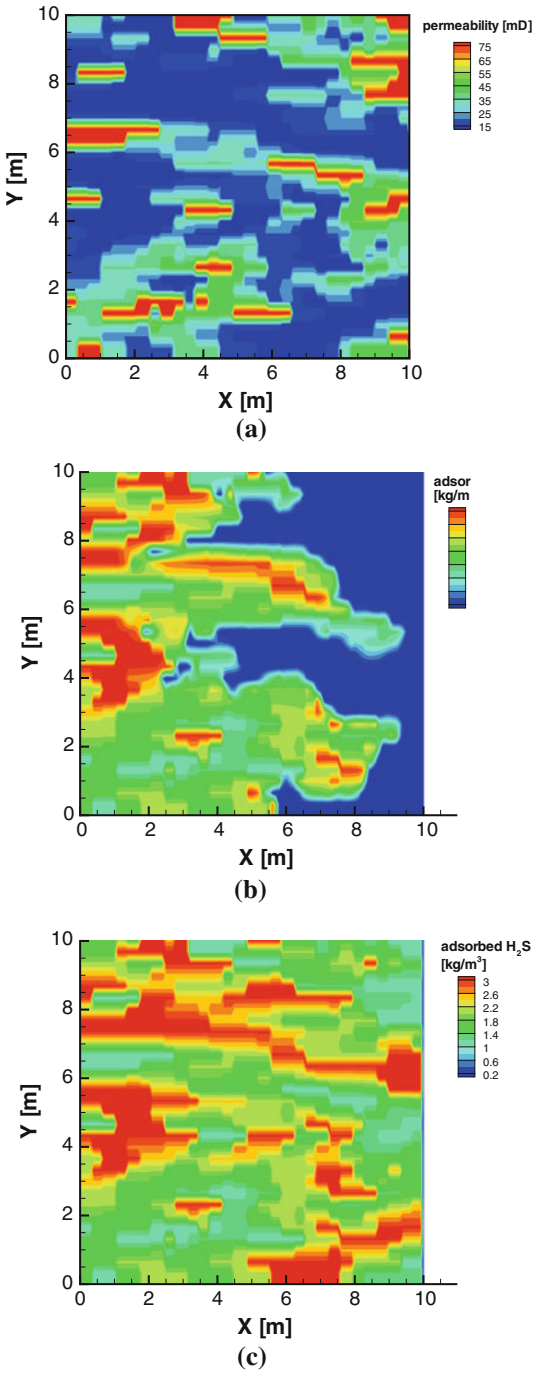

Fig. 7 Comparison of permeability field and distribution of adsorbed H_2S at $t = 6$ days and $t = 20$ days. **a** Heterogeneous permeability field. **b** Distribution of abosrbed H_2S at $t = 6$ days. **c** Distribution of adsorbed H_2S $t = 20$ days

which most of the water flows, some H_2S reaches production earlier than in the standard case.

8 Concluding remarks

We have presented a model for the transport of hydrogen sulfide (H_2S) in oil reservoirs. Water containing dissolved

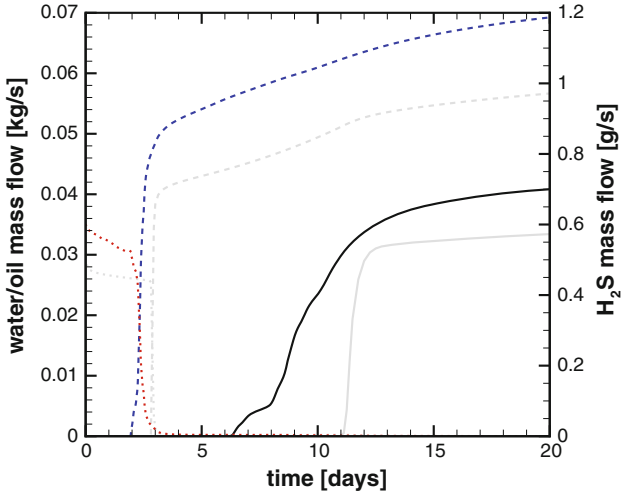

Fig. 8 Fluxes of oil, water and H_2S at production for heterogeneous permeability field shown in Fig. 7a, compared to the standard case. The *continous line* represents the H_2S flux, the *dashed line* is the water flux, and the oil flux is depicted with the *dotted line*. The results of the standard case simulation are shown in *gray*

H_2S is injected into an initially oil-filled, water-wet reservoir. The water breakthrough generally occurs before H_2S reaches production due to two retardation mechanisms: (1) mixing of H_2S with oil so that fractions remain in the residual oil and (2) adsorption of H_2S on the rock surface. An increase in residual oil saturation should result in later H_2S production, and a decrease should result in earlier H_2S production, as shown by simulations. An increase in the adsorption capacity of the rock is also shown to result in a later H_2S breakthrough. The breakthrough time also depends on the amount of injected H_2S as shown by simulation examples. Finally, a test example is given for the permeability–adsorption capacity relation.

Open Access This article is distributed under the terms of the Creative Commons Attribution Noncommercial License which permits any noncommercial use, distribution, and reproduction in any medium, provided the original author(s) and source are credited.

References

1. Bastian, P., Birken, K., Johannsen, K., Lang, S., Neuss, N., Rentz-Reichert, H., Wieners, C.: UG–a flexible software toolbox for solving partial differential equations. Comput. Vis. Sci. **1**(1), 27–40 (1997)
2. Bear, J.: Dynamics of Fluids in Porous Media. Dover Publications, New York (1988)
3. Chapoy, A., Mohammadi, A.H., Tohidi, B., Richon, D.: Estimation of water content for methane+ water and methane+ ethane+ n-butane+ water systems using a new sampling device. J. Chem. Eng. Data **50**(4), 1157–1161 (2005)
4. Class, H., Helmig, R., Bastian, P.: Numerical simulation of non-isothermal multiphase multicomponent processes in porous media. 1. An efficient solution technique. Adv. Water Resour. **25**(5), 533–550 (2002)

5. De Siqueira, A., Araujo, C.H., Reksidler, R., Pereira, M.: Uncertainty analysis applied to biogenic reservoir souring simulation. In: EUROPEC/EAGE Conference and Exhibition (2009)
6. Bryant, S.L., Sepehrnoori, K., Farhadinia, M.A., Delshad, M.: Development of a reservoir simulator for souring predictions. In: SPE Reservoir Simulation Symposium (2009)
7. Helmig, R.: Multiphase Flow and Transport Processes in the Subsurface a Contribution to the Modeling of Hydrosystems Environmental Engineering (Berlin). Springer, New York (1997)
8. Helmig, R., Braun, C., Emmert, M.: MUFTE: A Numerical Model for Simulation of Multiphase Flow Processes in Porous and Fractured Porous Media. Programmdokumentation (HG208) (1994)
9. Huber, R., Helmig, R.: Multiphase flow in heterogeneous porous media: A classical finite element method versus an implicit pressure-explicit saturation-based mixed finite element-finite volume approach. Int. J. Numer. Methods Fluids **29**(8), (1999)
10. Iliuta, I., Larachi, F.: Trickle bed mechanistic model for (non-) Newtonian power-law foaming liquids. Chem. Eng. Sci. **64**(8), 1654–1664 (2009)
11. Langmuir, I.: The constitution and fundamental properties of solids and liquids. II. Liquids. J. Am. Chem. Soc. **39**(9), 1848–1906 (1917)
12. Ligthelm, D.J., RB, Brint, J.F., Schulte, W.M.: Reservoir souring: an analytical model for H2S generation and transportation in an oil reservoir owing to bacterial activity. In Offshore Europe Conference, Aberdeen 3–6 September 1991 (1991)
13. Millington, R.J., Quirk, J.P.: Permeability of porous solids. Trans. Faraday Soc. **57**, 1200–1207 (1961)
14. Qin, G., Wang, H., Ewing, R.E., Espedal, M.S.: Numerical simulation of compositional fluid flow in porous media. Numerical Treatment of Multiphase Flows in Porous Media, pp. 232–243 (2000)
15. Sunde, E., Thorstenson, T., Torsvik, T., Vaag, J.E., Espedal, M.S.: Field-related mathematical model to predict and reduce reservoir souring. In: Proceedings of SPE International Symposium on Oilfield Chemistry, New Orleans (1993)